High Frequency Loss and Electromagnetic Field Distribution for Striplines and Microstrips

H. Louis Lo, *Member, IEEE*, J. Frank Kauffman, *Member, IEEE*, and Paul D. Franzon, *Member, IEEE*

***Abstract*— A new three-component measured equation of invariance (MEI) boundary condition is developed and applied to the hybrid edge/nodal vector finite element method. The electric field distribution on the cross section of various lossy transmission lines is calculated. The propagation constant of a lossy transmission line with coated conductor strip is also calculated. The three-component MEI boundary condition simulates the field distribution on the artificial boundary for electromagnetic field excited by the surface charge density and the three vector components of the electric current density. Numerical experiments are performed to test the method by comparing calculated transmission loss with the measured data.**

***Index Terms*— Finite element method, measured equation of invariance, microstrip, multichip module, package design, propagation mode, triplate strip.**

I. Introduction and Motivation

With rapid improvement in transistor switching speeds, the interconnections within and between integrated circuits (IC's) are increasingly limiting the performance of very large scale integration (VLSI) systems [1]. These fine interconnect lines are often complex structures containing multiple layers of dielectric and/or conductor materials. For example, many multichip module (MCM) technologies use clad copper interconnect structures, cables often use gold-coated conductors, and even IC interconnects are becoming heterogeneous.

Unfortunately, no current electromagnetic modeling technique can handle multilayer conductors. Computer-based modeling techniques are essential if we wish to evaluate multiple technology alternatives and to produce simulation models. In this paper, we extend the measured equation of invariance (MEI) boundary condition to handle such structures.

In order to calculate the electromagnetic field distribution accurately with limited computer resources, it is very important to choose an efficient numerical method with a suitable boundary condition to truncate the infinite space. The loss from the strip conductor in an MCM causes the electric field to be induced in the axial direction. Therefore, the field distribution for a wave propagating along a transmission line in an MCM is affected by the surface charge and axial electric field. The hybrid edge/nodal vector finite element method (VFEM) is designed to handle the lossy microstrip in an MCM, but its perfect conductor boundary condition which just assigns zero field on the boundary was used for this numerical method. There is no other boundary condition being used with the hybrid edge/nodal VFEM because the eigenvalue equation from hybrid edge/nodal VFEM is not compatible with the global boundary condition or any local boundary conditions other than perfect conductor boundary condition.

The MEI boundary condition is a simple local boundary condition. It is based on a linear finite difference equation for determining the electric field distribution on the boundary element. Because the MEI boundary condition incorporates the conductor geometry into the finite difference equation, the boundary condition can be placed very close to the conductor surface without sacrificing accuracy. The small calculated area for the numerical method with MEI boundary condition will reduce the size of the matrix equation for the calculation. Therefore, the current density distribution on the cross section contour of the conductor can be calculated with limited computer resources. But, prior to this work, the MEI boundary condition was used only for calculating two-dimensional (2-D) scattering of TE or TM waves [2], [3]. In this work, the theory of the MEI boundary condition is extended to the boundary condition for the hybrid edge/nodal VFEM for calculating the electric field distribution of a propagating wave in a transmission line in MCM.

This paper is organized as follows: The theory and the application of the three-component MEI boundary are discussed in Section II. The application of the three-component MEI boundary condition for the hybrid edge/nodal VFEM is explained in Section III. The calculated results are compared with measured results in Section IV. Finally, our conclusions are offered in Section V.

II. Theory and Modeling

The MEI boundary condition is based on a finite difference equation to describe how the electromagnetic field distribution on a boundary element relates to the field distribution on the neighboring elements. The finite difference equation is given as

$$\sum_{i=0}^{n-1} a_i \phi_i = 0 \tag{1}$$

where $i = 0$ corresponds to the boundary element and $i = 1, i = 2, \cdots, i = n-1$ correspond to the neighboring elements.

Manuscript received March 19, 1998; revised November 3, 1998. This paper was supported in part by DARPA under Contract DASH04-94-G-003-P2, an NSF Young Investigator Award, and a North Carolina Supercomputering Center Research Grant.

H. L. Lo is with Tyco Submarine Systems Ltd., Holmdel, NJ 07733 USA.

J. F. Kauffman and P. D. Franzon are with the Department of Electrical and Computer Engineering, North Carolina State University, Raleigh, NC 27695 USA.

Publisher Item Identifier S 1521-3323(99)00994-6.

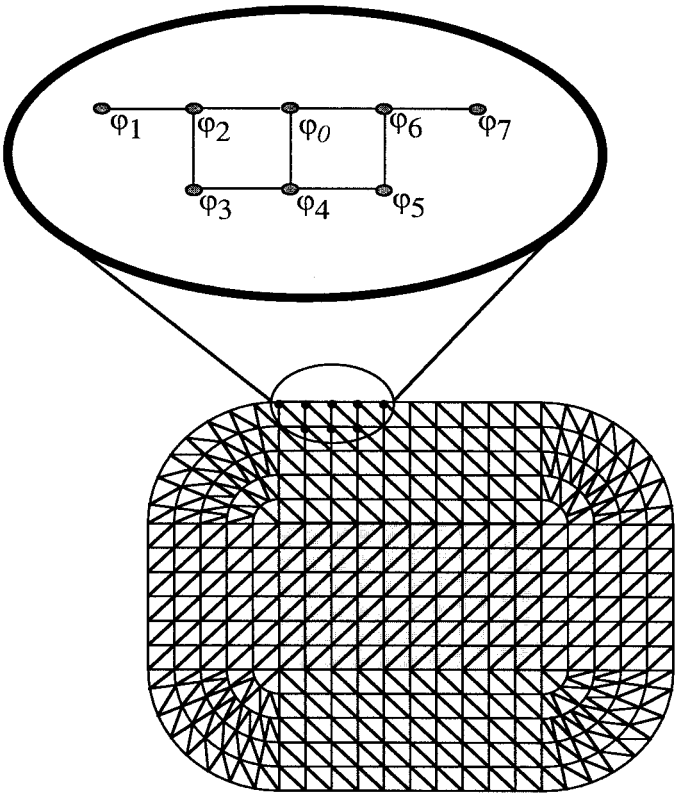

Fig. 1. The boundary cells for nodal field calculation.

Let $a_0 = -1$, and the coefficients $a_1, \cdots, a_{n-1}$ are determined by applying $n-1$ distributions (called metrons) [2] of surface current density on the conductor. The field distribution on the boundary element is determined by equation (1) instead of by the mesh equation from finite element method. The theory of MEI boundary condition is based on three postulates:

Postulate 1: The coefficients of (1) are location dependent.

Postulate 2: The coefficients of (1) are geometry specific.

Postulate 3: The coefficients of (1) are approximately invariant with excitation.

Postulates 1 and 2 explain why we can use MEI boundary to replace the whole outer space. Postulate 3 enables us to replace the outer boundary of FDM/FEM mesh cells by MEI cells as shown in Fig. 1.

Outside the conductor, the electric field in the axial direction is induced by the current inside the conductor, and the transverse electric field is mainly due to the surface charge on the conductor. In order to reduce the complication of the eigenvalue calculation for the propagation modes, we calculate the boundary condition of electric field in the axial direction independent with the electric field in the transverse direction.

A. MEI Boundary Condition for the Electric Field in the Axial Direction

In order to calculate the field distribution on the boundary nodes of the FEM mesh, eight-node cells are used as shown in Fig. 1. The axial component of the electric field outside the conductor is related to the electric current density in the conductor by the following relation:

$$\vec{E} = j\omega\vec{A} \tag{2}$$

with

$$\vec{A} = \frac{\mu_0}{4\pi}\int_S G(\vec{r}|\vec{r'})\, J(\vec{r'})\, d\vec{r'} \tag{3}$$

where S is the cross section of the conductor, μ_0 is the free space permeability, and $G(\vec{r}|\vec{r'})$ is the Green's function.

The direction of the electric field on each node is perpendicular to the cross section plane of the strip conductor, and the electric field on the nodes of a boundary cell is calculated by the axial component of the current density distribution in the conductor. By using a finite difference equation to represent the relationship of the field distribution on the nodes in a MEI cell, the field distribution on the boundary node is determined by the field distribution on its neighboring nodes.

For the eight-node MEI cells shown in Fig. 1, the axial component of electric field on node 0, E_0, is determined by the following finite difference equation:

$$\begin{aligned} &a_1E_1 + a_2E_2 + a_3E_3 + a_4E_4 \\ &+ a_5E_5 + a_6E_6 + a_7E_7 = E_0 \end{aligned} \tag{4}$$

where $a_1, \cdots, a_7$ are the coefficients of the finite difference equation, and the values must be calculated for each MEI cell. The variables $E_0, \cdots, E_7$ are the axial components of electric field on the nodes in a MEI cell, and their values are calculated by the axial component of current density distribution in the conductor. By using the equivalence principle [5], the effect of the current density distribution inside the conductor can be replaced by a current density distribution on the conductor surface. For an assigned current density distribution (*metron* k) on the surface of the conductor, the axial component of electric field distribution on node i is

$$E_i^k(\vec{r}) = \oint_C G(\vec{r}|\vec{r'})J_z^k(\vec{r'})\, d\vec{r'} \tag{5}$$

where C is the contour of the conductor, $J_z^k(\vec{r'})$ is the surface current density of *metron* k at point $\vec{r'}$ on the surface of the conductor, and $G(\vec{r}|\vec{r'})$ is the Green's function. For the infinite transmission line, the Green's function is the Hankel function of zero order and second kind [3].

Seven metrons are needed to derive the coefficients $a_1, \cdots, a_7$ in (4). The electric field distribution on node 0, node $1, \cdots$, node 7 is calculated by (5) for each assigned metron. After substituting the electric field on the nodes in (4) by applying seven different metrons, *metron* $0, \cdots$, *metron* 6 on the conductor surface, we get 7 equations as

$$\sum_{j=1}^{7} a_j E_j^i = E_0^i, \qquad i = 0, 1, \cdots, 6 \tag{6}$$

where E_i^j, calculated by (5), is the electric field intensity on node i due to *metron* j.

The coefficients $a_1, \cdots, a_7$ can be determined by Solving the linear equations in (6). Therefore, the electric field distribution on node 0 is determined by (4), and this boundary

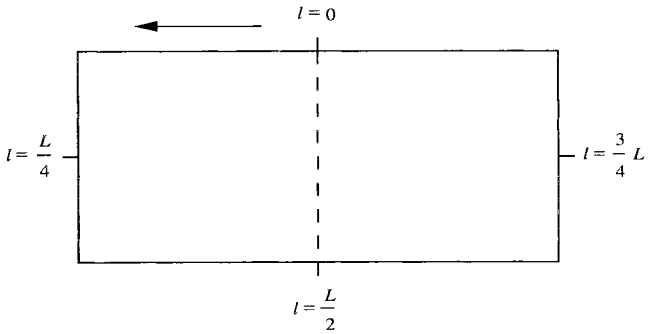

Fig. 2. The position l on the periphery of the strip conductor.

condition is used to truncate the infinite space outside the calculated area.

In order to solve the coefficients, a_1 to a_7, in (4), seven different metrons of current density distribution on the conductor surface are needed. We define the length of the cross section contour of the conductor strip as L and the point on the cross section contour of the strip is l as shown in Fig. 2. Because the metron and the space derivative of the metron must be continuous functions [4], the seven distributions of surface current density in the axial direction are assigned as sinusoidal distributions

$$J_z^k(l) = \begin{cases} \cos\dfrac{2k\pi l}{L}, & k = 0,1,2,3 \\ \sin\dfrac{2(k-3)\pi l}{L}, & k = 4,5,6. \end{cases} \tag{7}$$

The axial current density on the conductor surface can be approximated by a summation of Fourier series

$$\begin{aligned} J_s &= \sum_{k=0}^{3} b_k \cos\frac{2k\pi l}{L} + \sum_{k=4}^{6} b_k \sin\frac{2(k-3)\pi l}{L} \\ &= \sum_{k=0}^{6} b_k J_z^k(l). \end{aligned} \tag{8}$$

The residuals of the MEI boundary equations for the the current distribution of the sinusoidal components in (8) are zero because we use these terms to evaluate the finite difference equation for the boundary condition. The use of the geometry specific Green's function for the metrons to calculate the coefficients of the finite difference equation makes the use of additional terms unnecessary. Mei *et al.* [2] have shown that the residuals of the boundary equations are almost zero for additional higher-order terms in the summation of (8).

B. MEI Boundary Condition for Transverse Electric Field

The boundary condition for the electric field due to the surface charge density is modeled using the MEI cells with perpendicular-edge elements, and the boundary condition for the electric field due to the surface current density on the transverse plane is modeled using MEI cells with parallel-edge elements as shown in Fig. 3 because the MEI boundary can be placed very close to the conductor surface. On the transverse plane, the electric field outside the conductor is determined both by the surface charge density on the conductor and the surface current density perpendicular to the axial direction. On the surface of the conductor, the direction of the electric field vector due to the surface charge density is perpendicular to the conductor surface, and the electric field due to the surface current density is parallel to the conductor surface. The edge elements of the numerical mesh in the dielectric are used to define the two orthogonal field components: the electric field perpendicular to the artificial boundary, and the electric field parallel to the artificial boundary.

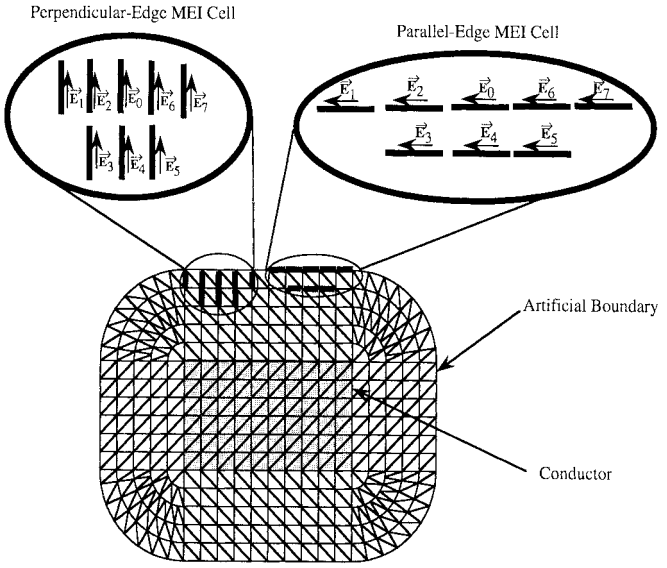

Fig. 3. The boundary cells for edge field calculation.

For a perpendicular-edge MEI cell in Fig. 3, the electric field $\vec{E}_0$ on the perpendicular-edge element 0 is determined by the following finite difference equation:

$$\begin{aligned} a_1\vec{E}_1 + a_2\vec{E}_2 + a_3\vec{E}_3 + a_4\vec{E}_4 \\ + a_5\vec{E}_5 + a_6\vec{E}_6 + a_7\vec{E}_7 = \vec{E}_0 \end{aligned} \tag{9}$$

where the coefficients, $a_1, \cdots, a_7$ are calculated by applying 7 metrons on the surface of the conductor. The value of the metron for surface charge density on the cross section contour of the conductor in Fig. 2 are assigned as

$$Q_s^k(l) = \begin{cases} \cos\dfrac{2k\pi l}{L}, & k = 0,1,2,3 \\ \sin\dfrac{2(k-3)\pi l}{L}, & k = 4,5,6 \end{cases} \tag{10}$$

where k is the metron number.

The electric field intensity on perpendicular-edge element i in Fig. 3 is due to the surface charge *metron* k as

$$\begin{aligned} \vec{E}_i^k(\vec{r}) &= [\nabla V_i^k(\vec{r})] \cdot \hat{s}_i \\ &= \nabla\left[\frac{1}{4\pi\epsilon_r\epsilon_0}\oint_C G(\vec{r}|\vec{r'})Q_s^k(\vec{r'})\,d\vec{r'}\right] \cdot \hat{s}_i \end{aligned} \tag{11}$$

where $V_i^k(\vec{r})$ is the electric potential on the perpendicular-edge element i, $Q_s^k(r')$ is the electric charge density on the conductor surface for *metron* k, ϵ_r is relative permittivity, ϵ_0 is the permittivity in free space, and $\hat{s}_i$ is an unit vector on edge i, whose direction is toward the artificial boundary.

After seven metrons in (10) are applied to the finite difference equation (9) for a perpendicular-edge MEI cell, the coefficients of the MEI cells can be solved as described in Section II-A. By the same argument for eight-node MEI cells, the electric field on the perpendicular-edge element 0 is determined by the finite difference equation (9) for the perpendicular-edge boundary condition. The electric field on each perpendicular-edge element on the artificial boundary is determined by the finite difference equation calculated from the MEI cell of this boundary element instead of the mesh equation from FEM.

For the parallel-edge MEI cells in Fig. 3, the parallel-edge element 0 is determined by the following finite difference equation:

$$\begin{aligned} &a_1\vec{E}_1 + a_2\vec{E}_2 + a_3\vec{E}_3 + a_4\vec{E}_4 \\ &\quad + a_5\vec{E}_5 + a_6\vec{E}_6 + a_7\vec{E}_7 = \vec{E}_0 \end{aligned} \tag{12}$$

where the coefficients, $a_1, \cdots, a_7$ are calculated by applying 7 metrons of transverse current density on the surface of the conductor. The metrons of the surface current density on the cross section of the conductor in Fig. 2 are assigned as

$$J_s^k(l) = \begin{cases} \cos\dfrac{2k\pi l}{L}, & k = 0,1,2,3 \\ \sin\dfrac{2(k-3)\pi l}{L}, & k = 4,5,6 \end{cases} \tag{13}$$

where k is the metron number.

The electric field intensity on the parallel-edge element i from a metron is calculated by

$$\vec{E}_i^k(\vec{r}) = \oint_C G(\vec{r}|\vec{r'})\vec{J}_s^k(\vec{r'}) \cdot \hat{s}_i \, d\vec{r'} \tag{14}$$

where $\hat{s}_i$ is the unit vector on edge i, whose direction is counterclockwise and parallel to the artificial boundary, and $\vec{J}_s^k(\vec{r'})$ is the conductor surface current density on the transverse plane for *metron* k.

After seven metrons in (13) are applied to the finite difference equation of the parallel-edge MEI cell, the coefficients of the MEI cells can be solved as described in Section II-A. Therefore, the electric field intensity on the parallel-edge element 0 is determined by (12) for the parallel-edge boundary condition. The electric field on each parallel-edge element on the boundary is determined by the finite difference equation calculated from the MEI cell of this boundary element instead of the mesh equation from FEM.

III. Hybrid Edge/Nodal VFEM With Three-Component MEI Boundary Condition

In a source-free lossy medium, the homogeneous vector Helmholtz's equation for the electric field is

$$\nabla \times (\nabla \times \vec{E}) - k_c^2\vec{E} = 0 \tag{15}$$

where the wave number k_c is a complex number for the conducting region

$$\begin{aligned} k_c &= \omega\sqrt{\mu_c\epsilon_c} \\ &= \omega\sqrt{\mu_r\mu_0\hat{\epsilon}_r\epsilon_0} \end{aligned} \tag{16}$$

where μ_r is the relative permeability of the region of interest, $\hat{\epsilon}_r$ is the complex relative permittivity of the region of interest, μ_0 and ϵ_0 are the permeability and permittivity in free space. Substituting (16) into (15), we get the vector Helmholtz's equation

$$\nabla \times (\nabla \times \vec{E}) - k_0^2\mu_r\hat{\epsilon}_r\vec{E} = 0 \tag{17}$$

where k_0 is the wave number in free space, and it equals to $\omega\sqrt{\mu_0\epsilon_0}$.

For a conductor, the electric field and the magnetic field are related according to the time-harmonic Maxwell's equation

$$\begin{aligned} \nabla \times \vec{H} &= \vec{J} + j\omega\epsilon_0\vec{E} \\ &= \sigma\vec{E} + j\omega\epsilon_0\vec{E} \\ &= (\sigma + j\omega\epsilon_0)\vec{E} \\ &= j\omega\left(1 - j\frac{\sigma}{\omega\epsilon_0}\right)\epsilon_0\vec{E} \end{aligned} \tag{18}$$

where $\vec{J}$ is the density of the conduction current, σ is the conductivity of the conductor, and ω is the radian frequency. In order to simplify (18), we define the complex relative permittivity of a conductor as

$$\hat{\epsilon}_r = 1 - j\frac{\sigma}{\omega\epsilon_0} \tag{19}$$

and for a lossy dielectric it can be written as

$$\hat{\epsilon}_r = \epsilon_r(1 - j\tan\delta) \tag{20}$$

where ϵ_r is the relative permittivity of the dielectric, and $\tan\delta$ is the loss tangent. For a lossless dielectric, the loss tangent is zero. The VFEM functional of the Helmholtz's equation on the 2-D cross section is given by

$$\begin{aligned} F &= \iint_\Omega [(\nabla \times (\nabla \times \vec{E}) - k_0^2\mu_r\hat{\epsilon}_r\vec{E}) \cdot \vec{E}^*] \, dx \, dy \\ &= \iint_\Omega [(\nabla \times \vec{E}) \cdot (\nabla \times \vec{E})^* - k_0^2\mu_r\hat{\epsilon}_r\vec{E} \cdot \vec{E}^*] \, dx \, dy \end{aligned} \tag{21}$$

where Ω is the calculated area on the cross section plane, and the superscript $*$ means the complex conjugate.

In order to apply VFEM to the field calculation, we assign a number of hybrid edge/nodal triangular cells to cover the cross section of the strip conductor, and the partition is illustrated in Fig. 4. The edge elements, $\{E_t\}$, of the VFEM cell on the right-hand side of Fig. 4 are $\vec{E}_{t_1}, \vec{E}_{t_2}$, and $\vec{E}_{t_3}$. The node elements, $\{E_z\}$, of the cell are $\vec{E}_{z_1}, \vec{E}_{z_2}$, and $\vec{E}_{z_3}$. The distribution of the electric field in the x, y, and z directions for the enclosed area of each cell is determined by the field strength of the edge/node elements in the cell as

$$E = \begin{bmatrix} E_x \\ E_y \\ E_z \end{bmatrix} = \begin{bmatrix} \{U\}^T\{E_t\}_e \\ \{V\}^T\{E_t\}_e \\ j\{N\}^T\{E_z\}_e \end{bmatrix} \tag{22}$$

where $\{U\}$ and $\{V\}$ are the shape-function sets for the edge elements, $\{N\}$ is the shape-function set for the node elements, T is the transpose operator for the vector, and j is the square root of -1. The factor j is used to time the shape function

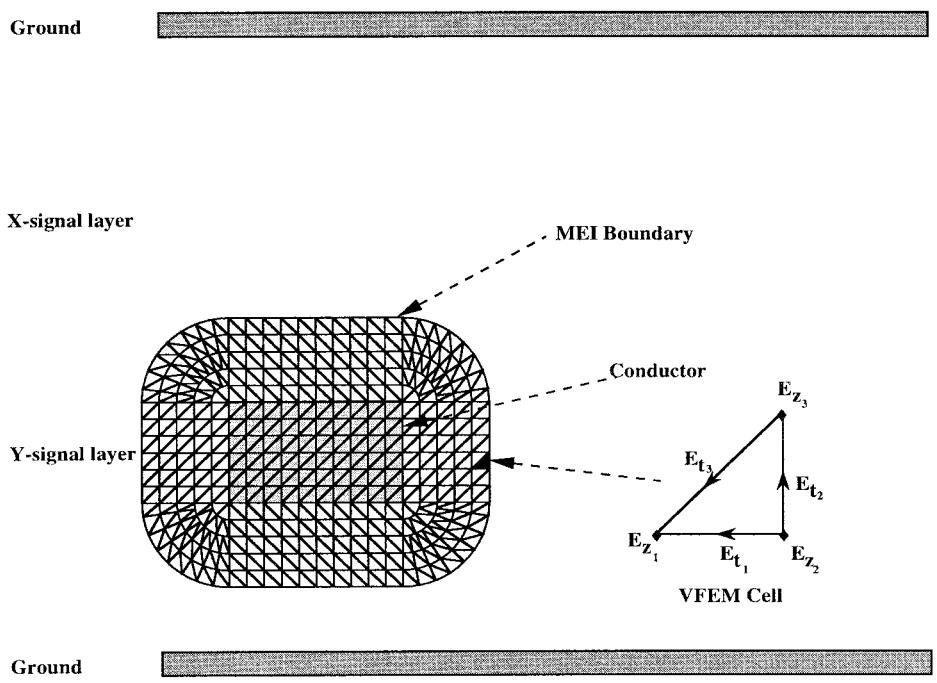

Fig. 4. The 2-D cross section of a stripline with triangular cells for VFEM calculation.

of node elements, because the field in the axial direction is perpendicular to the field in the transverse direction.

In order to get the electric field distribution on the finite element edges, we substitute (22) into (21), and minimize the VFEM functional by

$$\frac{\partial F}{\partial E_i} = 0, \qquad i = 1, 2, 3, \cdots, N \tag{23}$$

where N is the total number of edges. This results in the following matrix equation:

$$\begin{bmatrix} [K_{tt}] - \gamma^2[M_{tt}] & -\gamma[K_{tz}] \\ -\gamma[K_{zt}] & [K_{zz}] \end{bmatrix} \begin{bmatrix} \{E_t\} \\ \{E_z\} \end{bmatrix} = \begin{bmatrix} \{0\} \\ \{0\} \end{bmatrix}. \tag{24}$$

Separating the electric field strength into transverse and axial components in (24), we get the following matrix equations:

$$-[K_{tt}]\{E_t\} + \gamma[K_{tz}]\{E_z\} + \gamma^2[M_{tt}]\{E_t\} = \{0\} \tag{25}$$

$$\gamma[K_{zt}]\{E_t\} - [K_{zz}]\{E_z\} = \{0\}. \tag{26}$$

Eliminating the axial component from these two matrix equations, we get the following equation which is used to obtain the propagation constant γ

$$[K_{tt}]\{E_t\} - \gamma^2([K_{tz}][K_{zz}]^{-1}[K_{zt}] + [M_{tt}])\{E_t\} = \{0\}. \tag{27}$$

A. Applying Vector MEI Boundary Condition for the Elements in the Axial Direction

The boundary condition for the axial elements is to determine the field intensities of the elements on the artificial boundary by the MEI boundary equations instead of the hybrid edge/nodal VFEM mesh equations. In order to truncate the infinite open space, the MEI boundary equations are used to replace the node boundary elements in the axial direction in (26), and we get

$$\gamma[K'_{zt}]\{E_t\} - [K'_{zz}]\{E_z\} = \{0\}. \tag{28}$$

The ith row of matrix $[K'_{zt}]$ and $[K'_{zz}]$ in (28) contain the coefficients of a linear equation for calculating the electric field distribution of the ith element. In order to make the boundary elements in (28) become independent of the propagation constant, the rows of the boundary elements in the axial direction are assigned to zeros for matrix $[K'_{zt}]$. The rows of the boundary elements in the axial direction are replaced by the finite difference equations from the MEI boundary condition for matrix $[K'_{zz}]$. The electric field distribution on the boundary nodes is, therefore, determined by the finite difference equations which are obtained by truncating the infinite space by an artificial boundary—MEI boundary condition.

B. Applying Vector MEI Boundary Condition for the Elements in Transverse Direction

In order to truncate the open space for the hybrid edge/nodal VFEM calculation, we apply the MEI boundary condition for the edge elements on the boundary in (27) and get

$$[K'_{tt}]\{E_t\} - \gamma^2([K_{tz}][K_{zz}]^{-1}[K_{zt}] + [M_{tt}])'\{E_t\} = \{0\}. \tag{29}$$

We call (29) HTMEI equation with HTMEI standing for Hybrid edge/nodal FEM with the Three-component MEI Boundary Condition. The rows of the boundary elements in matrix $([K_{tz}][K_{zz}]^{-1}[K_{zt}] + [M_{tt}])'$ of (29) are set to zero for making the boundary condition independent of the propagation constant, γ. The rows of the boundary elements in matrix $[K'_{tt}]$ are replaced by the finite difference equations from the MEI boundary condition.

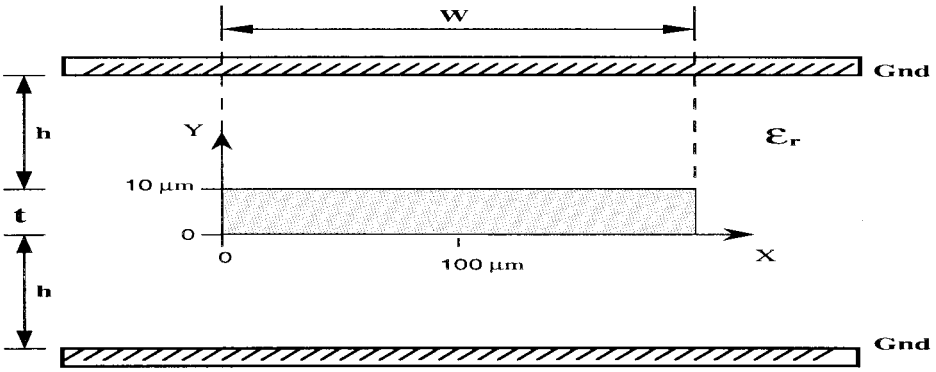

Fig. 5. The cross section of a triplate line.

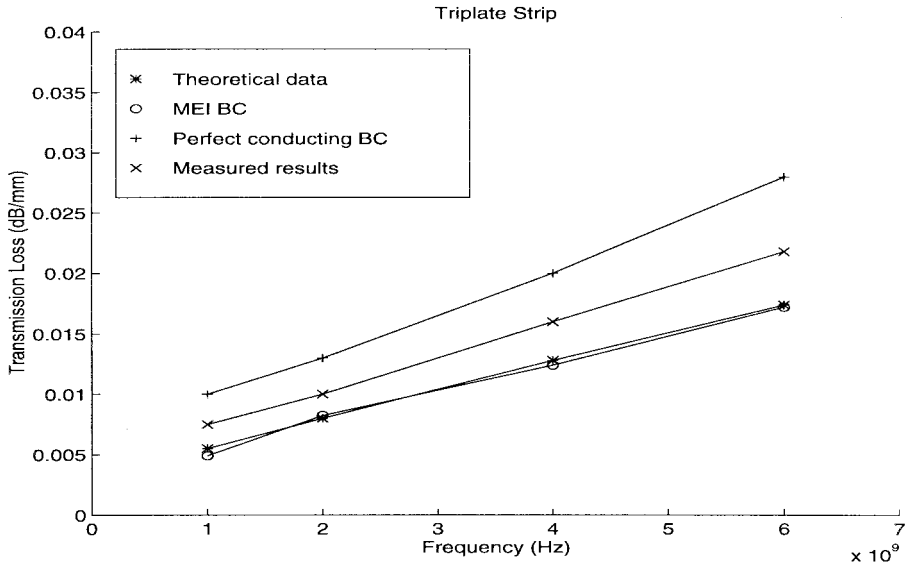

Fig. 6. Calculated and measured transmission loss versus frequency.

C. Eigenvalue Problem

In order to calculate the propagation mode of (27), we rewrite it as

$$A\{E_t\} - \lambda B\{E_t\} = \{0\} \tag{30}$$

with

$$A = [K'_{tt}]$$
$$B = ([K_{tz}][K_{zz}]^{-1}[K_{zt}] + [M_{tt}])'$$
$$\lambda = \gamma^2.$$

where γ is the complex propagation constant. Let $B\{E_t\} = y$, then $\{E_t\} = B^{-1}y$. Substituting $B\{E_t\}$ by y, and $\{E_t\}$ by $B^{-1}y$ in (30), we get

$$AB^{-1}y - \lambda y = \{0\} \tag{31}$$

Assigning $M = AB^{-1}$, we get an eigenvalue equation

$$My = \lambda y. \tag{32}$$

Since the matrix M is not sparse, we have no choice but to use a dense-matrix solver (QR decomposition) for calculating the complex eigenvalue. The solutions for the eigenvalues, $\lambda = \gamma^2$, in the eigenvalue equation represent the propagation modes. By substituting the eigenvalue of the dominant propagation mode back into (27), we calculate the transverse electric field distribution on the cross section of the stripline. The electric field distribution in the axial direction is calculated by substituting the eigenvalue of the dominant propagation mode and the transverse electric field distribution, $\{E_t\}$, into (26).

IV. Computational Results

We coded this method in Fortran and ran it on a Cray-YMP computer. In order to estimate the transmission loss and the electric field distribution in the conductor more accurately, the hybrid edge/nodal VFEM with the three-component MEI boundary condition is used to calculate the electric field distribution on the cross section of the transmission line. The boundary condition truncates the infinite space by a layer of boundary elements. The calculated results using edge/nodal VFEM with the three-component MEI boundary condition are close to the measured data at frequencies below 1 GHz. At high frequencies (>1 GHz), the conduction current density is concentrated in the area close to the conductor surface due to skin effect. Because the surface roughness of the conductor

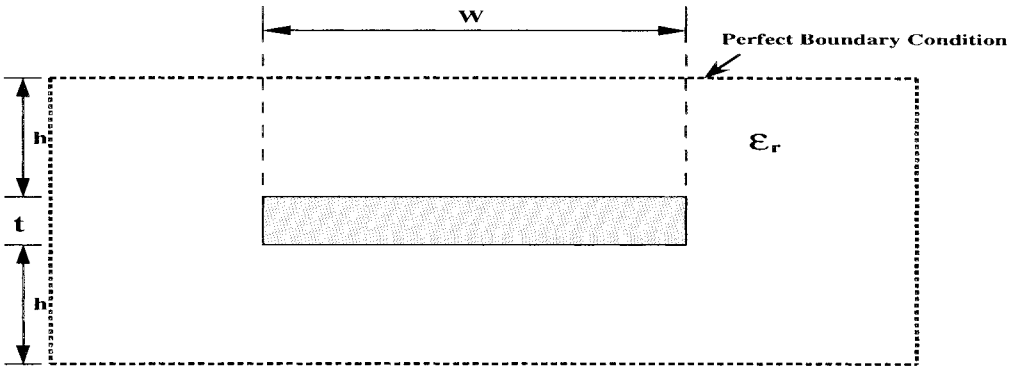

Fig. 7. The perfect conductor boundary condition on the cross section of the triplate line.

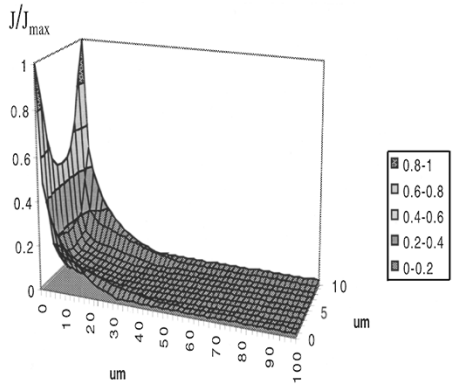

Fig. 8. The current density distribution on the cross section of the center strip of the triplate geometry at 2 GHz.

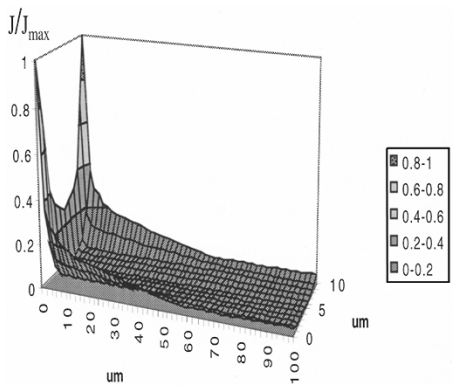

Fig. 9. The current density distribution on the cross section of the center strip of the triplate geometry at 4 GHz.

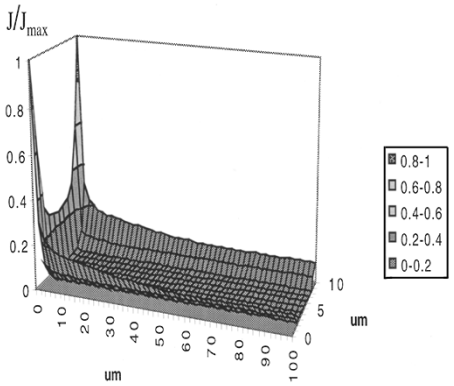

Fig. 10. The current density distribution on the cross section of the center strip of the triplate geometry at 6 GHz.

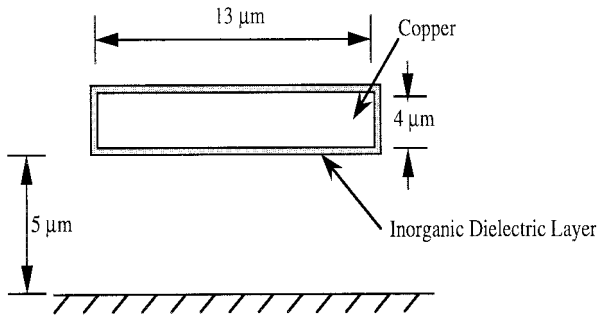

Fig. 11. The transmission line with a thin-film inorganic dielectric.

and the transmission loss from the ground are not included in the calculation, the measured data are somewhat higher than the calculated results at the higher frequencies. The calculated results can be used to choose the best structure for the transmission line to be used in the MCM without the cost of making samples, and for reducing the turn around time for improving performance.

A. The Triplate Strip Line

The hybrid edge/nodal VFEM with the three-component MEI boundary condition is used to calculate the transmission loss of a triplate strip. The cross section of the line is illustrated in Fig. 5. In order to compare the calculation results with the experimental data published by Taguchi *et al.* [6], the distance between two grounds, $2h+t$, is set to be 910 μm, the thickness of the conducting strip, t, 10 μm, and the width of the strip, w, 200 μm. For the dielectric, the relative dielectric constant, ϵ_r, is set to be 7.55, and the loss tangent, $\tan\delta$, is 0.005. The conductivity, σ, of the copper (reduction from CuO) is 2.5×10^7 S/m [6].

The transmission loss is a function of frequency as shown in Fig. 6. The theoretical values are simulated by HP85150 microwave design system (MDS). The results calculated by the hybrid edge/nodal VFEM with the three-component MEI boundary condition are close to the theoretical values which do not include the loss from the ground, but the results calculated by the edge/nodal VFEM with a wall of perfect conductor [7]

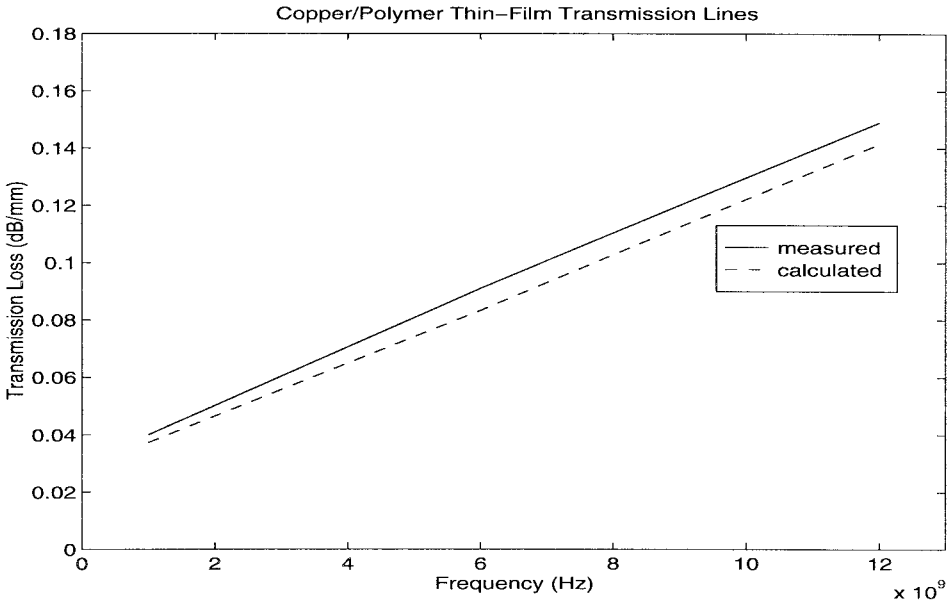

Fig. 12. The transmission loss versus frequency for the microstrip coated with a thin-film inorganic.

as its boundary condition are larger than the theoretical results and measured data. The perfect conductor boundary condition used in [7] is shown in Fig. 7. The measured data are higher than our calculated results, because our calculated results do not include the loss from ground plane. The three-component MEI boundary condition makes the field distribution in the dielectric close to the real situation, and improves the accuracy of the calculation.

In order to know how the current density distribution on the cross section of the conductor affects the transmission loss, we plot the current density distributions on the cross section of the conductor for different frequencies. For 2, 4, and 6 GHz, the current density distributions in the strip conductor are shown in Figs. 8–10. At high frequency, the current density distribution concentrates on the area close to the conductor surface, and the effective cross section area for conduction current is smaller than the effective cross section area at low frequency. Therefore, the transmission loss is larger for the higher frequency wave.

B. The Coated Interconnection Used in an MCM

The MCM manufacturers usually use copper as the conducting metal due to its low resistivity which provides these MCM technologies a distinct performance advantage at low cost. Polyimide is chosen as the dielectric material in the MCM package for its low dielectric loss. In order to eliminate the reaction between copper and polyimide [8], [9], a diffusion barrier layer between copper and polyimide is often added by the manufacturers. There are two barrier layers reported [10]: a thin film of inorganic dielectric and a thin film of metal. We used the structures published by Adema *et al.* [10] to calculate the propagation losses of the microstrip transmission lines and compare the calculated results with the measured data. The structures in Adema *et al.* [10] are: the microstrip clad with inorganic dielectric and the microstrip coated with chromium.

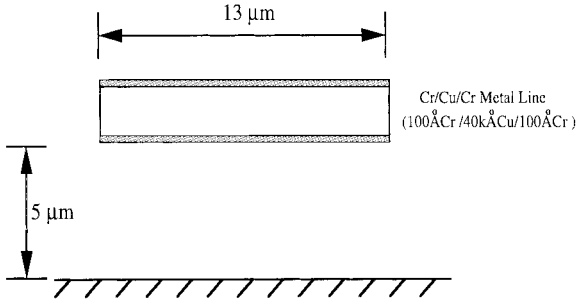

Fig. 13. The transmission line coated with a thin-film chromium.

For the microstrip structure shown in Fig. 11, the strip conductor is buried in the polyimide dielectric with a ground plane under it and the space above strip conductor is filled with polyimide. The strip conductor is copper clad with a thin film of inorganic dielectric. The dimensions of the structure are shown in Fig. 11. The thickness of the thin-film inorganic dielectric is much smaller than the thickness of the conductor. Because the transmission loss from the strip conductor is much larger than the loss from the inorganic dielectric, the electric properties of the inorganic dielectric are assumed the same as the electronic properties of polyimide to simplify the numerical calculation. The loss tangent of inorganic dielectric is assumed to be zero, and the relative dielectric constant, ϵ_r, is 3.0, which is the same as the relative dielectric constant of polyimide for the transmission loss calculation. The conductivity of copper for the strip conductor is 5.8×10^7 S/m.

The transmission loss of the inorganic dielectric clad microstrip is a function of frequency as shown in Fig. 12. The calculated transmission loss is smaller than the measured data because the transmission loss from the ground and the cladding dielectric is not included for the numerical calculation. At low frequency, the skin depth of the conductor is larger than the thickness of the conductor, the major transmission loss

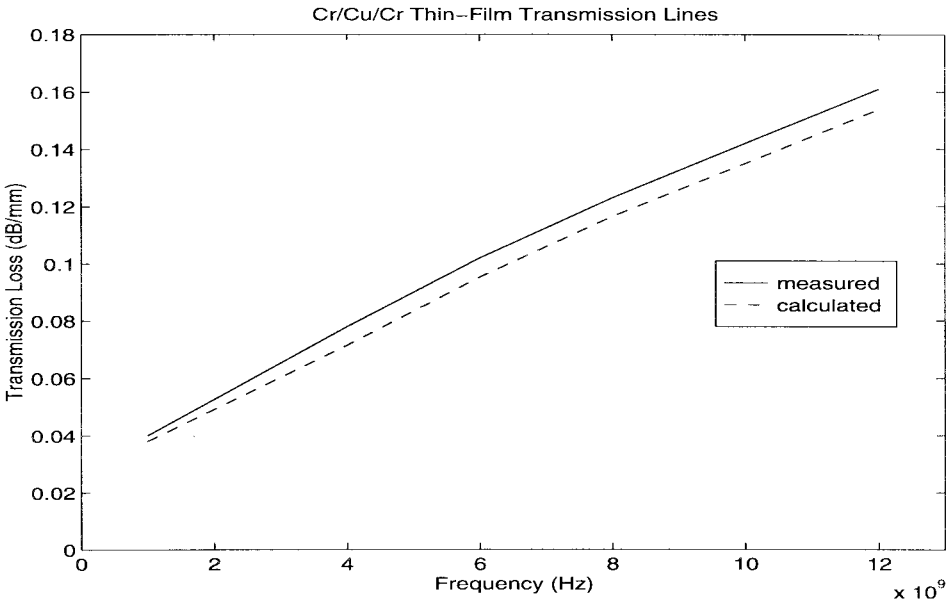

Fig. 14. The transmission loss of a transmission line coated with chromium.

comes from the strip conductor. Therefore, the difference of the transmission loss between the calculated results and the measured data is smaller at a lower wave frequency.

By using a Balzers BAK 760 electron-beam evaporator [10], the strip conductor is constructed of Cr/Cu/Cr with the thickness of 100 Å /4 μm/100 Å as shown in Fig. 13. The thickness and width of the copper conductor in Fig. 13 are the same as the copper conductor in Fig. 11 for comparing the transmission loss between these two microstrips. The conductivity of the copper is 5.8×10^7 S/m, but the conductivity of chromium is only 7.75×10^6 S/m.

As shown in Fig. 14, the calculated transmission loss is still lower than the measured data, and the difference between the calculated results and the measured data in Fig. 14 is smaller than the difference in Fig. 12. That's because the loss tangent of the clad inorganic dielectric in Fig. 11 is larger than the loss tangent of polyimide.

In order to choose the best transmission line structure for the system performance, we compare Fig. 14 with Fig. 12. The skin effect is not significant on the cross section of the conductor at low frequency, the difference between the transmission loss of the Cr/Cu/Cr microstrip and the transmission loss of the inorganic dielectric clad microstrip is small. As the frequency increases, the current density is higher in the area close to the bottom of the strip conductor. Because the resistivity of chromium is higher than the resistivity of copper, the transmission loss of the Cr/Cu/Cr microstrip is higher than the transmission loss of the inorganic dielectric clad microstrip for wave propagation at high frequency.

V. Conclusion

In this work, we developed the three-component MEI boundary condition for the hybrid edge/nodal VFEM. This three-component MEI boundary condition is applied to (27) formed by the three-dimensional (3-D) vector Helmholtz's equation in the transmission line, then a HTMEI (29) is formulated. By calculating the eigenvector of the lowest-mode eigenvalue of the HTMEI equation, we obtained the field distribution on the transverse plane. The square roots of the eigenvalues are the complex propagation constants. The real part of the propagation constant is the attenuation constant and the transmission loss can be calculated by the attenuation constant.

The boundary condition for the hybrid edge/nodal FEM is an approximate method for the field distribution calculation. The infinite space with the effect of the ground plate(s) is truncated by the three-component MEI cells for the boundary condition. The boundary condition is not only used to simulate the wave propagation in the open area, but also applied to hybrid edge/nodal FEM to calculate all the possible propagation modes. The finite difference equation of the MEI boundary condition is used to define the boundary elements for the calculation. We coded the technique to run on a Cray-YMP computer. Typical run times were 20 min.

The transmission loss consists of the loss from the strip conductor, the loss from the dielectric, the loss from the conductor surface roughness, and the loss from the ground. The calculated transmission loss of this paper includes the loss from the strip conductor and the loss from the dielectric. The trend of the calculated transmission loss is consistent with the trend of the measured transmission loss. The calculated transmission loss is 5–10% less than the measured transmission loss in general. The relatively small difference between the calculated and measured transmission losses suggests that the transmission loss is dominated by the loss from the strip conductor, and the loss from the dielectric.

References

[1] H. Hsieh, W. Liu, P. Franzon, and R. Cavin III, "Clocking optimization and distribution in digital systems with scheduled skews," *J. VLSI Signal Process. Syst.*, vol. 16, pp. 131–147, June 1997.

[2] K. Mei, R. Pous, Z. Chen, Y. Liu, and M. Prouty, "Measured equation of invariance: A new concept in field computation," *IEEE Trans. Antennas Propagat.*, vol. 42, pp. 320–327, Mar. 1994.
[3] A. C. Cangellaris and D. B. Wright, "Application of the measured equation of invariance to electromagnetic scattering by penetrable bodies," *IEEE Trans. Magn.*, vol. 29, pp. 1628–1631, Mar. 1993.
[4] K. K. Mei and Y. Liu, "Comments on 'a theory and numerical analysis of the measured equation of invariance'," *IEEE Trans. Antennas Propagat.*, vol. 43, pp. 1168–1171, Oct. 1995.
[5] R. F. Harrington. *Time-Harmonic Electromagnetic Fields*. New York: McGraw-Hill, 1961.
[6] Y. Taguchi, K. Miyauchi, K. Eda, and T. Ishida, "A GHz-band ceramic multi-layer substrate and its application to a hybrid IC," in *IEEE MTT-S Dig.*, June 1993, pp. 1325–1328.
[7] M. S. Alam, M. Koshiba, K. Hirayama, and Y. Hayashi, "Analysis of lossy planar transmission lines by using a vector finite element method," *IEEE Trans. Microwave Theory Tech.*, vol. 43, pp. 2466–2471, Oct. 1995.
[8] G. M. Adema, I. Turlik, L. Hwang, G. A. Rinne, and M. J. Berry, "Effects of polymer/metal interaction in thin-film multichip module applications," *IEEE Trans. Comp., Hybrids, Manufact. Technol.*, vol. 13, pp. 766–774, Dec. 1990.
[9] S. P. Kowalczyk, Y. H. Kim, G. F. Walker, and J. Kim, "Polyimid on copper: The role of solvent in the formation of copper precipitates," *Appl. Phys. Lett*, vol. 52, pp. 375–376, Feb. 1988.
[10] G. M. Adema, L. Hwang, and G. A. Rinne, "Passivation schemes for copper/polymer thin-film interconnections used in multichip modules," *IEEE Trans. Comp., Hybrids, Manufact. Technol.*, vol. 16, pp. 53–59, Feb. 1993.
[11] W. T. Week, L. L. Wu, M. F. McAllister, and A. Singh, "Resistive and inductive skin effect in rectangular conductors," *IBM J. Res. Develop.*, vol. 23, pp. 652–660, Nov. 1979.

H. Louis Lo (M'98) received the B.S. degree in electrical engineering from National Cheng-Kung University, Tainan, Taiwan, R.O.C., the M.S. degree in electrical engineering from the University of South Carolina, Columbia, in 1986, and the Ph.D. degree in electrical and computer engineering from North Carolina State University, Raleigh, in 1997.

From 1988 to 1994, he worked on electrical design of multichip packaging for Microelectronic Center North Carolina, Research Triangle Park, NC. He is a Senior Technical Staff Member in the Research and Development Department, Tyco Submarine Systems, Ltd., Holmdel, NJ. His research interests include modeling for interchip interconnection and circuit design for high-speed communication systems.

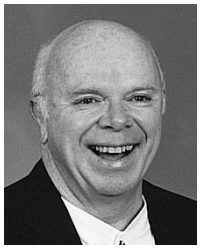

J. Frank Kauffman (S'65–M'70) was born in Princeton, MO, in 1937. He received the B.S.E.E. degree from the University of Missouri, Rolla, in 1960, the M.S.E.E. degree from the University of Illinois, Urbana, in 1964, and the Ph.D. degree from North Carolina State University, Raleigh, in 1970.

He has worked as an Electrical Engineer for Westinghouse Electric Corporation and Corning Glass, Ithaca, NY. He has been a member of the faculty of the Department of Electrical and Computer Engineering, North Carolina State University, since 1970, where he is a Professor.

Paul D. Franzon (S'85–M'88) is currently a Professor in the Department of Electrical and Computer Engineering at North Carolina State University. He has over eight years experience in electronic systems design and design methodology research and development. During that time, in addition to his current position, he has worked at AT&T Bell Laboratories, Holmdel, NJ, at the Australian Defense Science and Technology Organization, as a founding member of a successful Australian technology startup company, and as a consultant to industry, including technical advisory board positions. His current research interests include design sciences/methodology for high speed packaging and interconnect, for high speed and low power chip design and the application of microelectromechanical machines to electronic systems. In the past, he has worked on problems and projects in wafer-scale integration, IC yield modeling, VLSI chip design and communications systems design. He has published over 50 articles and reports. He is the co-editor and author on a book about multichip module technologies. His teaching interests focuses on microelectronic systems building including package and interconnect design, circuit design, processor design, and the gaining of hands-on systems experience for students.